Pergamon

0094-114X(95)00115-8

Mech. Mach. Theory Vol. 31, No. 7, pp. 891–911, 1996

0094-114X/96 $15.00 + 0.00

COMPUTERIZED DESIGN AND GENERATION OF CYCLOIDAL GEARINGS

FAYDOR L. LITVIN and PIN-HAO FENG

Department of Mechanical Engineering, University of Illinois at Chicago, Chicago, IL 60607, U.S.A.

(Received 9 November 1994; in revised form 7 September 1995)

Abstract—The generation and design of cycloidal (trochoidal) gearings that have found application in Wankel engine, Root's blowers and pumps are considered. The paper covers the following topics: (i) generation and geometry of planar cycloidal gearings and rotors of screw Root's blowers, and (ii) improved design that allows to avoid profile and surface singularities. Computer programs in support to proposed analytical solutions have been developed. Numerical examples that illustrate the developed theory are represented. Copyright © 1996 Elsevier Science Ltd

NOMENCLATURE

C—Center of the pin circle
O_i—Center of the centrodes
I—The instantaneous center of rotation
ρ_i—Radius of the pin circle
r_i—Radius of the centrodes
a—Distance between the center of the pin circle and the center of the centrode 1
θ, θ_i—Parameter of the generated curve
ϕ_i—Angle of gear rotation
ψ—Angle of rotation in the screw motion (Root's blower, Section 8)
p—Screw parameter (Root's blower, Section 8)
κ_2—Curvature of the generated curve
$\mathbf{r}_j^{(i)}$—Position vector of a point in coordinate system S_j
m_{21}—Gear ratio

1. INTRODUCTION

Cycloidal gears have initially found application as watch and clock gears. At present, such gears are applied in Wankel engine, pumps and Root's blowers (see Figs 1–4).

We consider a planar cycloidal gearing whose one link is provided with pin-teeth [1–3]. The profiles of the teeth of the mating link are curves that are conjugated to the pin-teeth (Figs 1 and 2). Conjugation of rotor 1 with chamber 2 (Fig. 3) is another example of a cycloidal gearing with pin-teeth applied in Wankel engine [4–7]. In this case the rotor (link 1) performs a planetary motion in two components: (i) the transfer motion, rotation about O_2 and (ii) the relative motion, rotation about O_1 (Fig. 3). The chamber (link 2) is at rest. Root's blower [1–3] is also an example of the discussed type of cycloidal gearing (Fig. 4). However, we have to consider in this case that the rotor's tooth (the lobe) has an addendum (it is the pin), and a dedendum whose profile is a curve conjugated with the circular arc of the addendum of the mating rotor. Figure 4(a) and 4(b) shows Root's blowers with two and three lobes, respectively.

In the case of gearings shown in Figs 1–3 the number N_1 of pins of the driving gear and the number N_2 of "teeth" of the driven gear must satisfy the relation [1]

$$N_1 - N_2 = 1$$

Therefore, the gear ratio is

$$m_{21} = \frac{N_1}{N_2} = \frac{N_1}{N_1 - 1}$$

In the case of a Root's blower we have that $N_2 = N_1$, and $m_{21} = 1$.

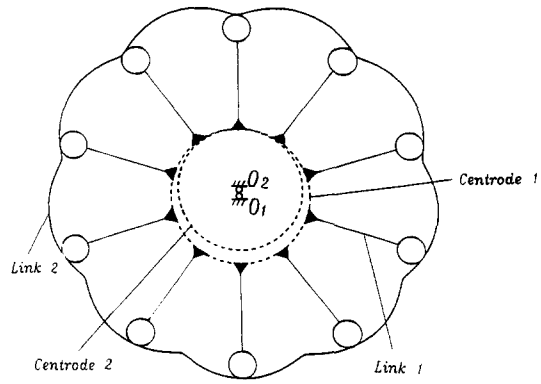

Fig. 1. Planar cycloidal gearing with pin teeth and internal tangency.

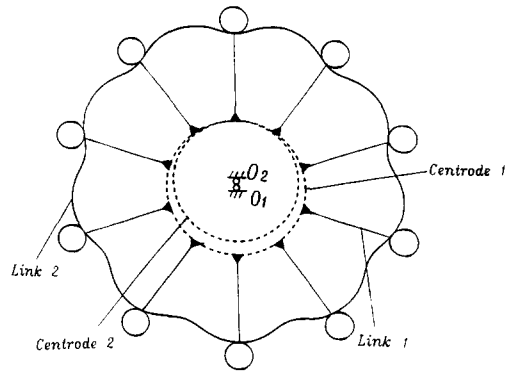

Fig. 2. Planar cycloidal gearing with pin teeth and internal tangency.

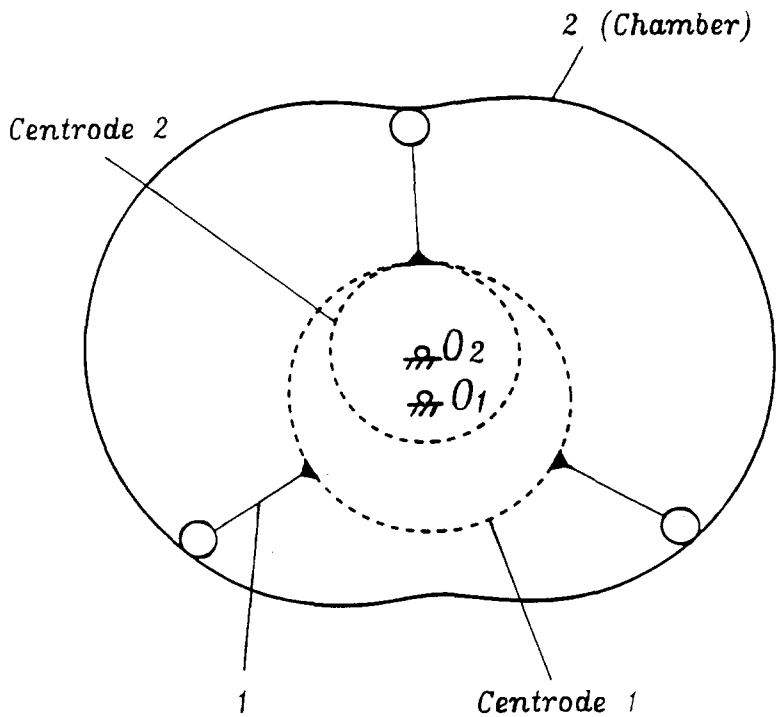

Fig. 3. Wankel's chamber and rotor.

Several scientists have performed research in the area of cycloidal gearings. Beard *et al.* [5, 8, 9] have investigated the cycloidal gearing applied in Wankel engine. Litvin [1–3] has investigated the meshing of Root's blowers and watch gears. Colbourne [10] has considered the geometry of trochoid envelopes. Sakun [11] has investigated the meshing of screw rotors applied in compressors.

A general approach for the computerized design and generation of planar cycloidal gearings is proposed in this paper. The contents of this paper cover the following topics:

(1) Determination of equations of cycloidal profiles of gear teeth.

(2) Investigation of the "behavior" of the contact normal (its orientation) during the process of meshing.

(3) Determination of the curvature of cycloidal profiles, and relations between the design parameters that correspond to positive and negative curvatures of the profiles, of a stationary point (when the curvature reaches its extreme value), and conditions that allow to avoid singularities of the generated profiles.

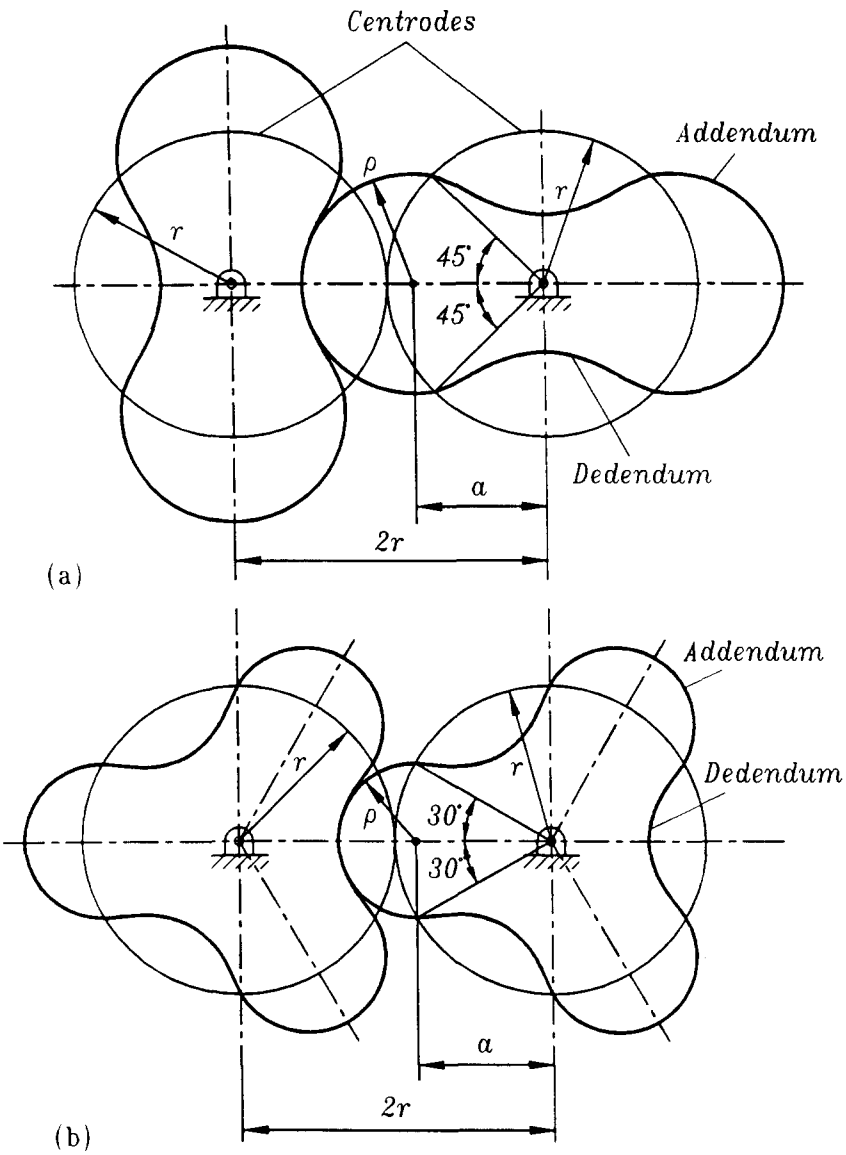

Fig. 4. Schematic of Root's blowers.

(4) A modified method for generation of chambers of Wankel engines by application of a tool with an increased diameter has been proposed.

(5) The design and meshing of screw rotors of Root's blower is considered as well. An improved design for avoidance of surface singularities has been developed.

The developed theory is illustrated with numerical examples and complemented with developed computer programs.

Special attention has been paid to application of the most effective methods of theory of gearing [1–3] to the investigation of discussed cycloidal gearings.

2. GENERATION OF TROCHOIDAL (CYCLOIDAL) CURVES

2.1. Applied coordinate systems

We consider a mechanism formed by two movable links and a fixed link, the frame of the mechanism. Coordinate systems S_1, S_2 and S_f are rigidly connected to links 1, 2 and f, respectively. The movable links perform rotation about parallel axes with a constant ratio of angular velocities. Henceforth, we will consider two cases when the rotation is performed in the same, or opposite

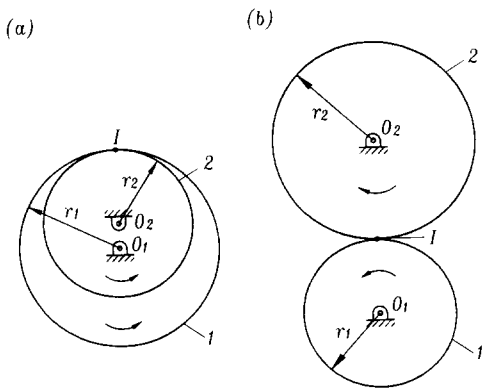

Fig. 5. Centrodes.

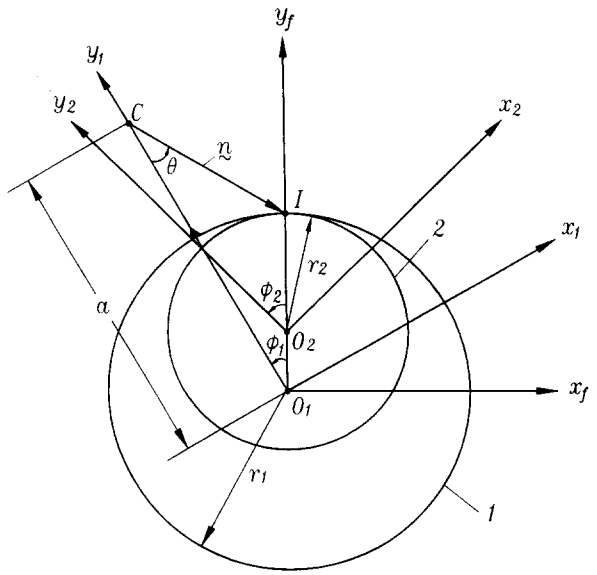

Fig. 6. For generation of trocoidal curve.

directions, respectively. The centrodes of the movable links are two circles of radii r_1 and r_2 that are in internal or external tangency as shown in Fig. 5.

2.2. *Equation of trochoidal curve*

We consider initially the case when the trochoidal curve is generated in coordinate system S_2 by point C that is rigidly connected to coordinate system S_1 (Fig. 6). The rotation of links 1 and 2 is performed in the same direction, the centrodes of links 1 and 2 are circles of radii r_1 and r_2, that are in internal tangency. Point I is the instantaneous center of rotation. Point C is represented in S_1 as

$$\mathbf{r}_1^{(c)} = [0 \quad a \quad 0]^{\mathrm{T}} \tag{1}$$

The trochoidal curve (designated as σ_2) is represented in S_2 by the following matrix equation

$$\mathbf{r}_2(\phi) = M_{21}(\phi)\mathbf{r}_1^{(c)} \tag{2}$$

Here: $\phi \equiv \phi_1$ is the generalized parameter of motion.

$$\frac{\phi_2}{\phi_1} = \frac{r_1}{r_2} = m_{21} \tag{3}$$

where m_{21} is the gear ratio. In this particular case we have that $m_{21} = \omega^{(2)}/\omega^{(1)}$ is constant.

Matrix

$$M_{21}(\phi) = \begin{bmatrix} \cos(\phi_1 - \phi_2) & -\sin(\phi_1 - \phi_2) & 0 & -(r_1 - r_2)\sin\phi_2 \\ \sin(\phi_1 - \phi_2) & \cos(\phi_1 - \phi_2) & 0 & -(r_1 - r_2)\cos\phi_2 \\ 0 & 0 & 1 & 0 \\ 0 & 0 & 0 & 1 \end{bmatrix} \tag{4}$$

describes the coordinate transformation from S_1 to S_2.

Equations from (2) to (4) represent the generated curve in parametric form, and ϕ is the variable parameter.

2.3. *Curvature of generated curve* σ_2

We may determine the curvature of curve σ_2 (it is generated by point C) using the following two approaches:

Approach 1. The curvature of a parametric curve represented by vector equation $\mathbf{r}_2(\phi)$ is determined by the equation [3]

$$\kappa_2 = \frac{\mathbf{r}_{\phi\phi} \cdot \mathbf{n}}{\mathbf{r}_\phi^2} \tag{5}$$

where

$$\mathbf{r}_{\phi\phi} = \frac{\partial^2 \mathbf{r}_2}{\partial \phi^2} \tag{6}$$

$$\mathbf{n} = \frac{\mathbf{k} \times \mathbf{r}_\phi}{|\mathbf{r}_\phi|} \left(\mathbf{r}_\phi \equiv \frac{\partial \mathbf{r}_2}{\partial \phi}, \quad \mathbf{k} \equiv \mathbf{k}_2 \right) \tag{7}$$

$\mathbf{n}$ is the unit normal to the generated curve; $\mathbf{k}_2$ is the unit vector of axis z_2 that is perpendicular to plane (x_2, y_2), where curve σ_2 is located.

The final expression for the curve curvature is

$$\kappa_2 = \frac{\mathbf{r}_{\phi\phi} \cdot (\mathbf{k} \times \mathbf{r}_\phi)}{|\mathbf{r}_\phi|^3} \tag{8}$$

After transformations of equation (8), we are able to represent the curvature of the curve by the following equation

$$\kappa_2 = \frac{-(m_{21} - 1)\lambda^2 - m_{21} + (2m_{21} - 1)\lambda \cos \phi}{r_1 (m_{21} - 1)(\lambda^2 - 2\lambda \cos \phi + 1)^{3/2}} \tag{9}$$

where $\lambda = a/r_1$.

The positive (negative) curvature shows that the curvature center is located on the positive (negative) direction of the normal or the unit normal that is determined with equation (7).

Approach 2. This approach is based on representation of the generated curve σ_2 in two-parameter form with an additional relation between the parameters. Curve σ_2 is represented in S_2 by the following equations

$$\mathbf{r}_2(\phi, \theta), \quad f(\phi, \theta) = 0 \tag{10}$$

The advantage of this approach is the possibility to visualize the orientation of the normal to the generated curve, the "behavior" of the normal in the process for generation, and develop an alternative approach for derivation of the curve curvature.

The upcoming derivations are based on the following procedure.

Step 1: Normal $\overline{CI}$ to the curve passes through the instantaneous center of rotation I (Fig. 6). The unit normal to the curve is represented in coordinate systems S_1 and S_2 as follows

$$\mathbf{n}_1 = [\sin \theta \quad -\cos \theta \quad 0]^T \tag{11}$$

$$\mathbf{n}_2 = \mathbf{L}_{21}(\phi)\mathbf{n}_1 \tag{12}$$

where $\mathbf{L}_{21}$ that represents the direction cosines is the 3×3 submatrix of M_{21}, and θ is measured from $\overline{O_1 C}$ in the counterclockwise direction (Fig. 6).

Step 2: The procedure of computations of $\mathbf{n}_2$ and the curve curvature requires the derivation of equation

$$f(\theta, \phi) = 0 \tag{13}$$

that relates parameters (θ, ϕ). This derivation is based on the consideration that the velocity $\mathbf{v}^{(12)}$ in relative motion is directed along the tangent to curve σ_2, and therefore we have

$$\mathbf{N} \cdot \mathbf{v}^{(12)} = \mathbf{n} \cdot \mathbf{v}^{(12)} = 0 \tag{14}$$

where $\mathbf{N}$ and $\mathbf{n}$ are the normal and the unit normal to σ_2, respectively. The scalar product in equation (14) is invariant with respect to the applied coordinate systems, and therefore we can represent equation (14) as

$$\mathbf{N}_i \cdot \mathbf{v}_i^{(12)} = \mathbf{n}_i \cdot \mathbf{v}_i^{(12)} = 0 \quad (i = 1, 2, f) \tag{15}$$

The subscript "i" in equation (15) indicates the coordinate system S_i where the vectors of the scalar product are represented. In the following derivations we will choose $i = 1$.

The relative velocity $\mathbf{v}_1^{(12)}$ is represented as [1–3]

$$\mathbf{v}_1^{(12)} = (\boldsymbol{\omega}_1^{(1)} - \boldsymbol{\omega}_1^{(2)}) \times \mathbf{r}_1 - (\overline{O_1 O_2}) \times \boldsymbol{\omega}_1^{(2)} = \omega_1(m_{21} - 1)\begin{bmatrix} a - r_1 \cos\phi \\ r_1 \sin\phi \\ 0 \end{bmatrix} \tag{16}$$

where $m_{21} = \omega^{(2)}/\omega^{(1)}$ is the ratio of angular velocities.

Equations (11), (15), and (16) yield that

$$f(\theta, \phi) = r_1 \sin(\theta + \phi) - a \sin\theta = 0 \tag{17}$$

Step 3: Curve σ_2 and the unit normal to the curve are represented in coordinate system S_2 by the following equations

$$\mathbf{r}_2(\phi) = M_{21}(\phi)\mathbf{r}_1^{(c)}, \quad \mathbf{n}_2(\theta, \phi) = \mathbf{L}_{21}(\phi)\mathbf{n}_1(\theta), \quad f(\theta, \phi) = 0 \tag{18}$$

Equations (18) represent in coordinate system S_2 the trochoidal curve generated by point C and the unit normal to the curve by two related parameters θ and ϕ.

Similarly, we can represent the generated curve σ_2 when the rotation of links 1 and 2 is performed in opposite directions.

Step 4: The investigation of equation (17) shows that the relation between parameters (θ, ϕ) depends on the ratio a/r_1.

Differentiating equation (17), we obtain that

$$\frac{d\theta}{d\phi} = \frac{\cos(\theta + \phi)}{\lambda \cos\theta - \cos(\theta + \phi)} \tag{19}$$

where $\lambda = a/r_1$.

Using equations (17) and (19), we obtain after transformations the following alternative equation

$$\frac{d\theta}{d\phi} = \frac{\lambda \cos\phi - 1}{\lambda^2 - 2\lambda \cos\phi + 1} \tag{20}$$

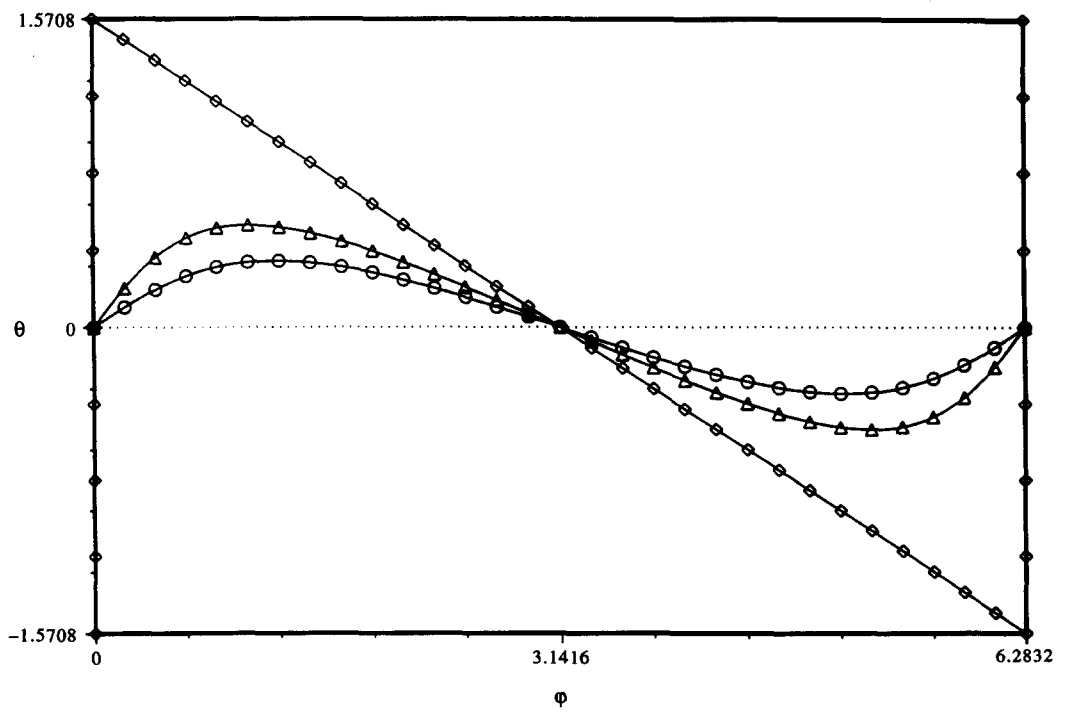

Fig. 7. Functions $\theta(\phi)$ for various coefficients $\lambda = a/\rho$: $\diamond \rightarrow \lambda = 1$, $\triangle \rightarrow \lambda = 2$, $\bigcirc \rightarrow \lambda = 3$, $\rho/r = 0.1333$.

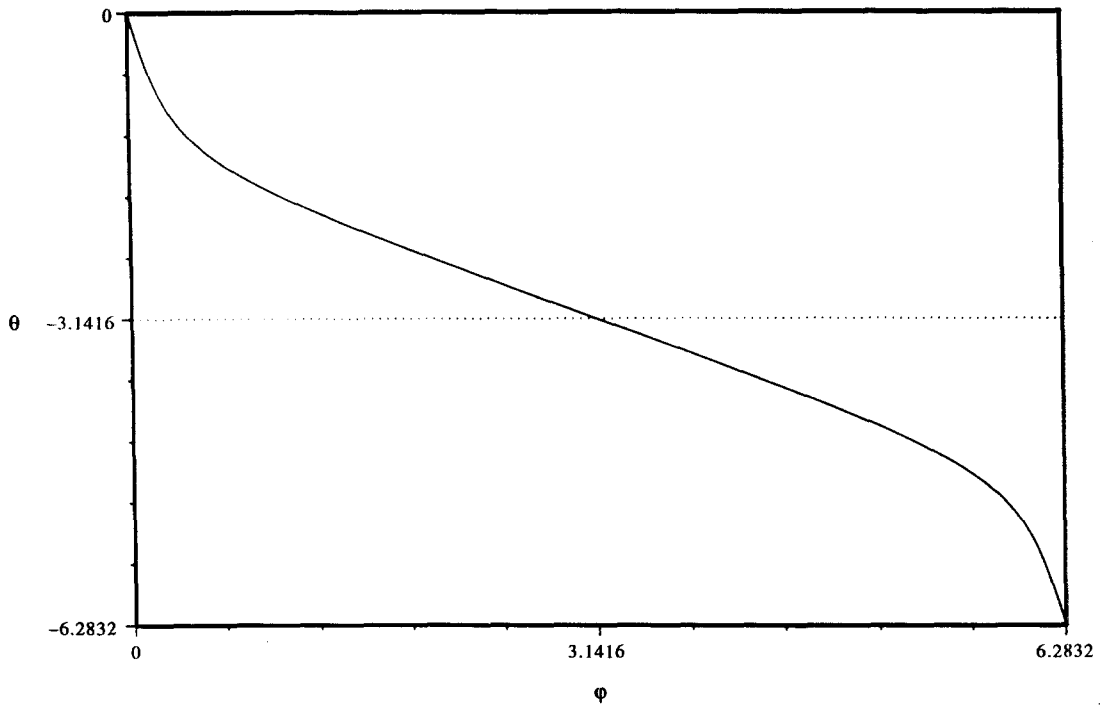

Fig. 8. Functions $\theta(\phi)$ for $\lambda = 0.8$, $\rho/r = 0.1333$.

At the position determined as

$$\cos\phi = |\sin\theta| = \frac{1}{\lambda} \quad (\lambda > 1) \tag{21}$$

we obtain that angle θ will reach its maximal value, and the speed of the normal $\overline{CI}$ with respect to position vector $\overline{O_1C}$ becomes equal to zero.

Figures 7 and 8 show the relation between θ and ϕ for the cases when $a/r_1 \geqslant 1$, and $a/r_1 < 1$, respectively. Figure 9 shows the two branches of the curve that is generated by point C when $a = r_1$. The common point of the branches is singular.

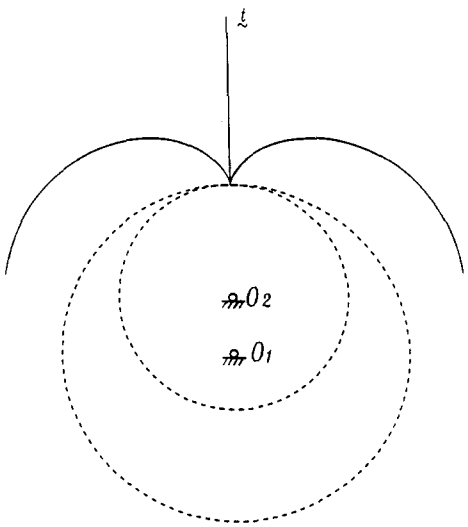

Fig. 9. Two branches of trochoidal curve with singularity point.

Step 5: The determination of the curvature of the generated curve represented in two-parameter form is based on the equation [1–3]

$$\kappa_2 \mathbf{v}_r^{(2)} = -\dot{\mathbf{n}}_r^{(2)} \tag{22}$$

where $\mathbf{v}_r^{(2)}$ is the velocity of the contact point that moves over σ_2, and $\dot{\mathbf{n}}_r^{(2)}$ is the velocity of the tip of the unit normal (in addition to the translational motion of $\mathbf{n}^{(2)}$) that moves over σ_2. In the discussed case $\mathbf{v}_r^{(2)} \equiv \mathbf{v}^{(12)}$ that is represented in S_1 by equation (16). Vector $\dot{\mathbf{n}}_r^{(2)}$ is represented in S_1 by the equation [1–3]

$$\dot{\mathbf{n}}_{r1}^{(2)} = \dot{\mathbf{n}}_{r1}^{(1)} + \boldsymbol{\omega}_1^{(12)} \times \mathbf{n} = \left[\frac{d\theta}{dt} + \frac{d\phi}{dt}(1 - m_{21})\right][\cos\theta \quad \sin\theta \quad 0]^T \tag{23}$$

After transformations, we obtain the following equations for determination of κ_2.

$$r_1 \sin(\theta + \phi) - a \sin\theta = 0$$

$$\kappa_2 = -\frac{[(1 + m_{21})a \cos\theta - r_1 m_{21} \cos(\theta + \phi)] \cos\theta}{(m_{21} - 1)(a - r_1 \cos\phi)[r_1 \cos(\theta + \phi) - a \cos\theta]}$$

$$= -\frac{[(1 + m_{21})a \cos\theta - r_1 m_{21} \cos(\theta + \phi)] \sin\theta}{(m_{21} - 1) r_1 \sin\phi [r_1 \cos(\theta + \phi) - a \cos\theta]} \tag{24}$$

Using the relations

$$\sin\theta = \frac{\sin\phi}{(\lambda^2 - 2\lambda \cos\phi + 1)^{1/2}} \tag{25}$$

$$\cos\theta = \frac{\lambda - \cos\phi}{(\lambda^2 - 2\lambda \cos\phi + 1)^{1/2}} \tag{26}$$

we obtain after transformations that equations (24) yield equation (9) for κ_2.

3. DETERMINATION OF CURVE Σ_2 CONJUGATED TO PIN-TOOTH

The applied coordinate systems (Fig. 10) are the same as shown in Fig. 6. The pin-tooth is a circle of radius ρ. The goal is to determine the curve that is conjugated to the pin-tooth.

Cycloidal gears shown in Figs 1 and 2 are applied in planetary trains when a high gear ratio of the train is required. This requirement can be observed if the planetary train is designed as a

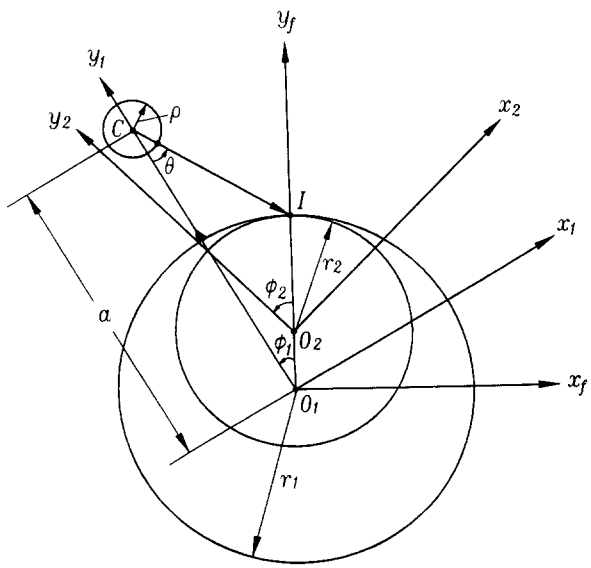

Fig. 10. For generation of a curve conjugated to a pin-tooth.

set of at least two pairs of cycloidal gears shown in Figs 1 and 2 and because the difference of number of teeth of the gears is equal to one. Theoretically, all pins of one gear in such a train can be in tangency with the teeth of the mating gear, but under the load only half of the teeth share the load. The pin teeth enter into mesh in sequence. The determination of the trochoidal curve as conjugate to the pin-tooth circle must be determined in the range of $\phi = 2\pi/N_1$, where N_1 is the number of pins, ϕ is the angle of rotation of the gear provided with pins.

The profile of the chamber of Wankel engine (Fig. 3) is a trochoidal curve that must be determined in the range $\phi = 2\pi m$, where m is a whole value that depends on the ratio m_{21}.

The determination of the trochoidal curve is based on the following procedure:

Step 1: We represent in parametric form the equation of the pin circle (designated by σ_1) by vector equation $\mathbf{r}_1(\theta)$.

Step 2: We derive the equation of meshing that provides the relation between parameters θ and ϕ.

Step 3: Using the coordinate transformation from S_1 to S_2, we represent in S_2 the family of pin circles. Considering simultaneously the family of pin circles and the equation of meshing, we may determine the curve that is conjugate to the pin circle.

The following is the detailed explanation of the mentioned above procedure.

3.1. Parametric representation of pin circle Σ_1

Using the drawings of Fig. 10, we represent the pin circle and its normal by the equations

$$\mathbf{r}_1(\theta) = [\rho \sin\theta \quad a - \rho\cos\theta \quad 0 \quad 1]^T \tag{27}$$

$$\mathbf{n}_1(\theta) = [\sin\theta \quad -\cos\theta \quad 0]^T \tag{28}$$

Angle θ, if positive, must be measured as shown in Fig. 10.

3.2. Representation of family of Σ_1 in S_2

Using the coordinate transformation from S_1 to S_2, we obtain

$$\mathbf{r}_2(\theta, \phi) = M_{21}(\phi)\mathbf{r}_1(\theta) \tag{29}$$

where $M_{21}(\phi)$ is represented by equation (4).

3.3. Equation of meshing

There are three alternative approaches for determination of equation of meshing.

(1) Approach 1 (applied in differential geometry) that is based on the equation

$$\frac{\partial \mathbf{r}_2}{\partial\theta} \times \frac{\partial \mathbf{r}_2}{\partial\phi} = 0 \tag{30}$$

(2) Approach 2 (applied in theory of gearing) that is represented as

$$\mathbf{n}_1 \cdot \mathbf{v}_1^{(12)} = \mathbf{N}_1 \cdot \mathbf{v}_1^{(12)} = 0 \tag{31}$$

(3) Approach 3 (based on Lewis' theorem). We use in this approach the theorem that the normal to Σ_1 at the point of tangency of Σ_1 and Σ_2 passes through the instantaneous center of rotation I. Thus, we have

$$\frac{X_1(\phi) - x_1(\theta)}{n_{x_1}(\theta)} = \frac{Y_1(\phi) - y_1(\theta)}{n_{y_1}(\theta)} \tag{32}$$

Here $X_1(\phi)$ and $Y_1(\phi)$ represent in S_1 the coordinates of point I, the instantaneous center of rotation.

Using any of the mentioned above approaches, we obtain that the equation of meshing coincides with the previously derived equation (17). Thus, we have

$$f(\theta, \phi) = r_1 \sin(\theta + \phi) - a \sin\theta = 0$$

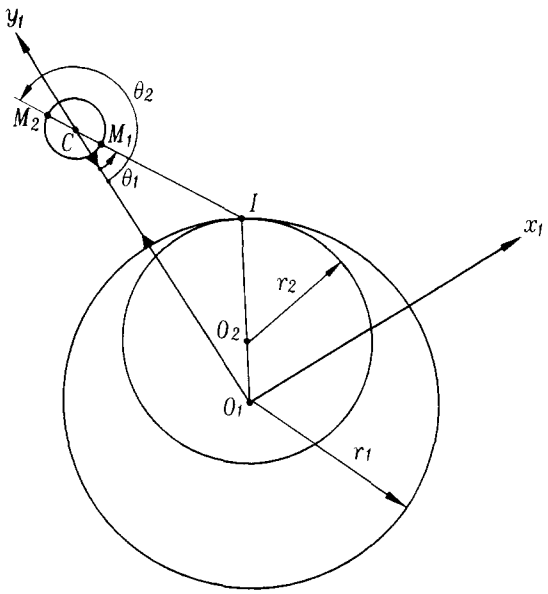

Fig. 11. Relation between parameters θ_1 and θ_2 for two envelopes.

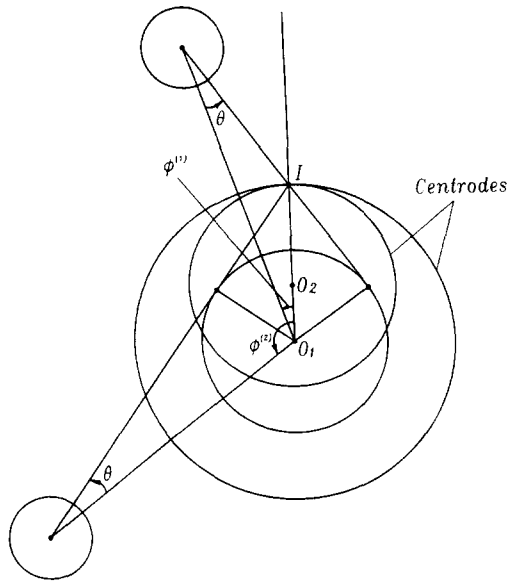

Fig. 12. Two positions of the pin with the same value of parameter θ.

It is easy to verify that equation of meshing provides two solutions for θ considering as given ϕ. Using this equation, we obtain that

$$\tan\theta = \frac{\sin\phi}{\lambda - \cos\phi} \quad \left(\lambda = \frac{a}{r_1}\right) \tag{33}$$

Equation (33) provides two solutions for θ that differ for 180°. This means that two envelopes exist at any instant (excluding the case when $a = r_1$ and $\phi = 0$, see below). The geometric interpretation of this statement is illustrated with Fig. 11. The drawings show that when the normal to the pin passes through the instantaneous center of rotation I, the pin may have two contact points with Σ_2: M_1 and M_2.

The relation between parameters θ and ϕ of equation of meshing (17) depends on the ratio a/r_1 (see Figs 7 and 8). In the case of $a/r_1 > 1$, the working part of the pin circle is an arc, and during the process of meshing the contact points perform a reciprocative motion over the circular arc. At the position determined with $|\sin\theta| = \cos\phi = 1/\lambda$ [see equation (21)] the velocity of the contact point in its motion over the pin circle is zero.

It is important to recognize that in the case of $\lambda > 1$, two values of ϕ correspond to the same value of θ (with an exception when $\theta = \theta_{max}$). This means that there are two positions of the driving link when the same pin point generates in sequence two respective points of the conjugate profile as shown in Fig. 12. Drawings of this figure yield that

$$\phi^{(2)} + \phi^{(1)} = 180° - 2\theta$$

where $\phi^{(2)}$ and $\phi^{(1)}$ designate the related positions of the driving link.

3.4. Equations of the envelope

The envelope Σ_2 to the family of pin circles is determined with equations (29) and (17) considered simultaneously.

4. CURVATURE OF CURVE Σ_2

The curvature of curve Σ_2 may be determined by application of two approaches: (i) as the curvature of the curve that is equidistant to curve σ_2 (see Section 2), and (ii) using the direct

relations between the curvatures of the pin circle Σ_1 and the generated curve Σ_2 [1–3]. The second approach requires the application of the following three relations [1–3]:

$$\dot{\mathbf{n}}_r^{(2)} = \dot{\mathbf{n}}_r^{(1)} = \boldsymbol{\omega}^{(12)} \times \mathbf{n}^{(1)} \tag{34}$$

$$\mathbf{v}_r^{(2)} = \mathbf{v}_r^{(1)} + \mathbf{v}^{(12)} \tag{35}$$

$$f_\theta \frac{d\theta}{dt} + f_\phi \frac{d\phi}{dt} = 0 \tag{36}$$

Here:

$$\dot{\mathbf{n}}_r^{(1)} = \frac{d\theta}{dt} [\cos\theta \quad \sin\theta \quad 0] \tag{37}$$

$$\mathbf{v}_r^{(1)} = \rho \frac{d\theta}{dt} [\cos\theta \quad \sin\theta \quad 0] \tag{38}$$

$$f_\theta \frac{d\theta}{dt} + f_\phi \frac{d\phi}{dt} = [a\cos\theta - r_1\cos(\theta+\phi)]\frac{d\theta}{dt} - r_1\cos(\theta+\phi)\frac{d\phi}{dt} = 0 \tag{39}$$

The results of investigation are as follows:

(1) Applying the first approach and using equation (9), we obtain that the curvature κ_2 of curve Σ_2 is represented by the equation

$$\frac{1}{\kappa_2} = \frac{r_1(m_{21}-1)(\lambda^2 - 2\lambda\cos\phi + 1)^{3/2}}{-(m_{21}-1)\lambda^2 - m_{21} + (2m_{21}-1)\lambda\cos\phi} \mp \rho \tag{40}$$

where the upper and lower signs correspond to the internal and external tangency of the pin circle with the envelope. It is assumed that the centrodes are in internal tangency [Fig. 5(a)].

(2) An inflection point of curve $\Sigma_2 = 0$ means such a point of the curve where $\kappa_2 = 0$. The analysis of equation (40) is based on following considerations:

(i) $1/\kappa_2 \to \infty$ if

$$-(m_{21}-1)\lambda^2 - m_{21} + (2m_{21}-1)\lambda\cos\phi = 0 \tag{41}$$

(ii) Equation (41) yields that

$$\cos\phi = \frac{m_{21} + (m_{21}-1)\lambda^2}{(2m_{21}-1)\lambda} \tag{42}$$

Here ϕ determines the position of link 1 when an inflection point of Σ_2 (if such a point exists) is generated; $\lambda = a/r_1$.

(iii) It follows from equation (42) that an inflection point exists indeed if

$$\frac{m_{21} + (m_{21}-1)\lambda^2}{(2m_{21}-1)\lambda} \leqslant 1 \tag{43}$$

Then we obtain the following requirement for λ

$$1 \leqslant \lambda \leqslant \frac{m_{21}}{m_{21}-1} \tag{44}$$

(iv) It is obvious that if

$$\lambda > \frac{m_{21}}{m_{21}-1} \tag{45}$$

curve Σ_2 is a convex one. Curve Σ_2 is a convex–concave one if inequality (44) is satisfied, and curve Σ_2 has an inflection point.

(3) A stationary point of curve Σ_2 means such a point where the curvature radius is of an extreme value [12] and

$$\frac{d}{d\phi}\left(\frac{1}{\kappa_2}\right) = 0 \tag{46}$$

Equations (46) and (40) yield that a stationary point exists at positions where

$$\sin\phi[(2-m_{21})\lambda^2+(2m_{21}-1)\lambda\cos\phi-(m_{21}+1)]=0 \tag{47}$$

It follows from equation (47) that stationary points of curve Σ_2 exist at positions determined by

$$\sin\phi=0 \tag{48}$$

and

$$\cos\phi=\frac{(m_{21}-2)\lambda^2+m_{21}+1}{(2m_{21}-1)\lambda} \tag{49}$$

The curvature radius at the positions $\phi=0$ and $\phi=180^\circ$ is determined by the following equations

$$\frac{1}{\kappa_2}=\frac{r_1(m_{21}-1)(\lambda\mp1)^2}{\pm m_{21}-(m_{21}-1)\lambda}\mp\rho \tag{50}$$

The upper and lower signs of the fraction part in equation (50) correspond to positions $\phi=0$ and $\phi=180^\circ$, respectively. In the case when curve σ_2 is considered (it is generated by point C, see Fig. 6), we have to take in equations (50) that $\rho=0$.

Equation (49) provides the third stationary point if ϕ is changed in the range $0\leqslant\phi\leqslant\pi$. The curvature radius of Σ_2 at the stationary position is determined with the equation

$$\frac{1}{\kappa_2}=-\frac{(m_{21}-1)\sqrt{27(a^2-r_1^2)}}{(2m_{21}-1)^{3/2}}\mp\rho \tag{51}$$

5. SINGULARITIES OF Σ_2

The normal to the generated curve Σ_2 at a singular point is indefinite, and Σ_2 may have at such a point two branches. Curve Σ_2 with singular points is unacceptable for application, such points must be avoided, and this can be achieved by proper relations between the design parameters.

A singular point on Σ_2 will occur if the velocity $\mathbf{v}_r^{(2)}$ of the contact point in its motion over Σ_2 becomes equal to zero [1–3]. Using the relations between the velocities of the contact point in its motions over Σ_1 and Σ_2, we will obtain the following relation [1–3]

$$\mathbf{v}_r^{(2)}=\mathbf{v}_r^{(1)}+\mathbf{v}^{(12)}=0 \tag{52}$$

The procedure of derivation of singularities is as follows:

Step 1: We represent equation (52) in coordinate system S_1

$$\frac{dx_1}{d\theta}\frac{d\theta}{dt}=-v_{x1}^{(12)},\quad \frac{dy_1}{d\theta}\frac{d\theta}{dt}=-v_{y1}^{(12)} \tag{53}$$

Step 2: Differentiating equation of meshing (17), we obtain

$$\frac{\partial f}{\partial\theta}\frac{d\theta}{dt}=-\frac{\partial f}{\partial\phi}\frac{d\phi}{dt} \tag{54}$$

Step 3: Equations (53) and (54) represent a system of three linear equations in one unknown $d\theta/dt$. The augmented matrix is

$$\begin{bmatrix} \dfrac{\partial x_1}{\partial\theta} & -v_{x1}^{(12)} \\ \dfrac{\partial y_1}{\partial\theta} & -v_{y1}^{(12)} \\ \dfrac{\partial f}{\partial\theta} & -\dfrac{\partial f}{\partial\phi}\omega^{(1)} \end{bmatrix} \tag{55}$$

and a solution for $d\theta/dt$ exists if the rank of matrix (55) is one. This requirement yields

$$(a - \rho \cos\theta - r_1 \cos\phi)(m_{21} - 1) + \rho \cos\theta \frac{d\theta}{d\phi} = 0 \tag{56}$$

Equations (56) and (17), if considered simultaneously, enable to determine the limiting value of ρ to avoid singularities on Σ_2.

Step 4: The closed form solution for the limiting value of ρ (considering as known m_{21}, r_1 and a), when singular points occur, is based on following considerations:

(i) We have obtained in Sections 2 and 3 that

$$\tan\theta = \frac{\sin\phi}{\lambda - \cos\phi}\left(\lambda = \frac{a}{r_1}\right) \tag{57}$$

and

$$\frac{d\theta}{d\phi} = \frac{(\lambda \cos\phi - 1)\cos^2\theta}{(\lambda - \cos\phi)^2} = \frac{\lambda \cos\phi - 1}{\lambda^2 - 2\lambda \cos\phi + 1} \tag{58}$$

(ii) We transform equation (56) as follows

$$\rho^2 = \frac{r_1^2(\lambda - \cos\phi)^2(m_{21} - 1)^2}{\cos^2\theta\left(\frac{d\theta}{d\phi} + 1 - m_{21}\right)^2} \tag{59}$$

Then, using equations (57), (58) and (59), we obtain

$$\rho^2 = \frac{r_1^2(m_{21} - 1)^2(c - d\cos\phi)^3}{(e + f\cos\phi)^2} \tag{60}$$

where

$$c = \lambda^2 + 1; \quad d = 2\lambda; \quad e = \lambda^2(1 - m_{21}) - m_{21}; \quad f = (2m_{21} - 1)\lambda \tag{61}$$

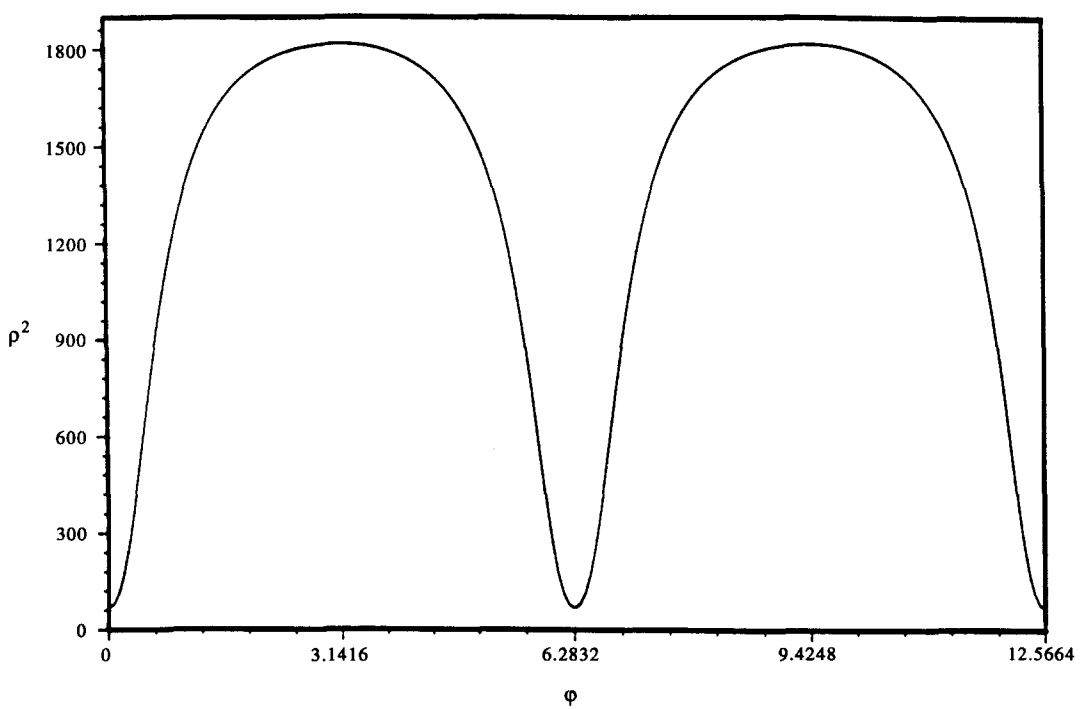

Fig. 13. For derivation of singularities: $\lambda = 0.8$.

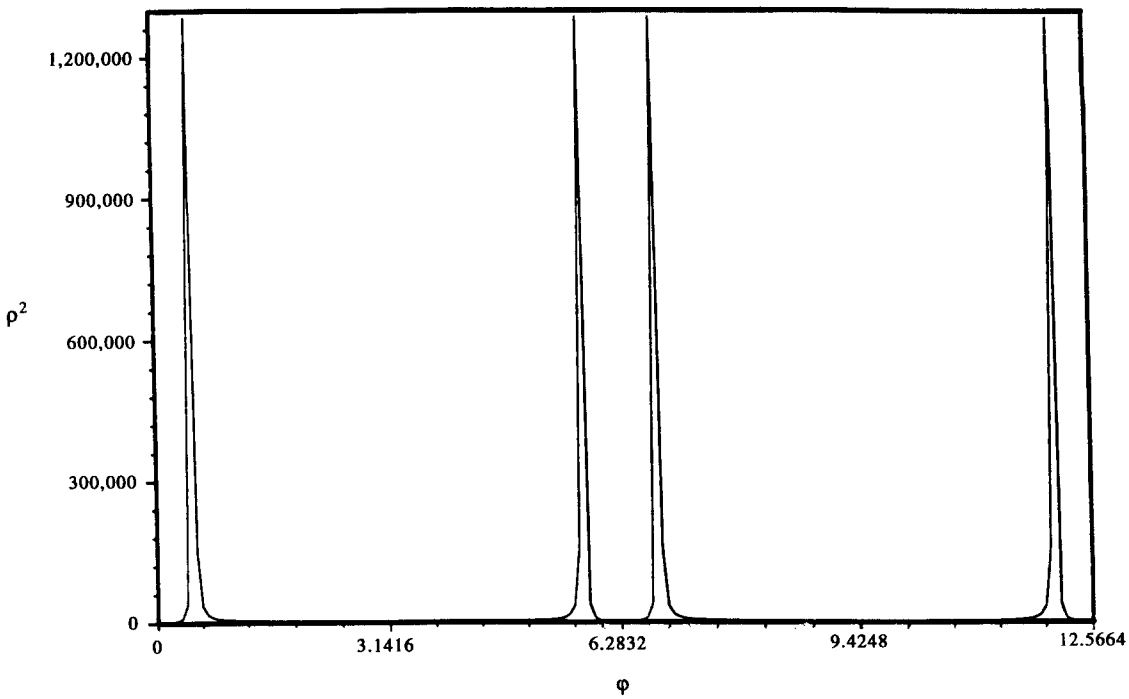

Fig. 14. For derivation of singularities: $\lambda = 1.5$.

(iii) Functions $\rho^2(\phi)$ for various coefficients of λ are shown in Figs 13 and 14. The extreme values of this function we may obtain considering that

$$\frac{d\rho}{d\phi} = \frac{r_1^2(m_{21}-1)^2 \sin\phi(c - d\cos\phi)^2(3de + 2cf + df\cos\phi)}{2\rho(e + f\cos\phi)^3} = 0 \tag{62}$$

The extreme values occur if: (i) $\sin\phi = 0$, (ii) $c - d\cos\phi = 0$, or (iii) $3de + 2cf + df\cos\phi = 0$. Using the drawings of Figs 13 and 14, we obtain that the minimum extreme value of ρ occurs when $\phi = 2n\pi$ (n is an integral). Therefore, the limiting value of ρ [see equation (61)] can be determined by

$$\rho^2 = \frac{r_1^2(m_{21}-1)^2(a-b)^3}{(c+d)^2} \tag{63}$$

Examples of singularities of the generated curve are shown in Fig. 15. To avoid the singularity occurred on the generated curve, we have to choose ρ^2 larger than provided by equation (63).

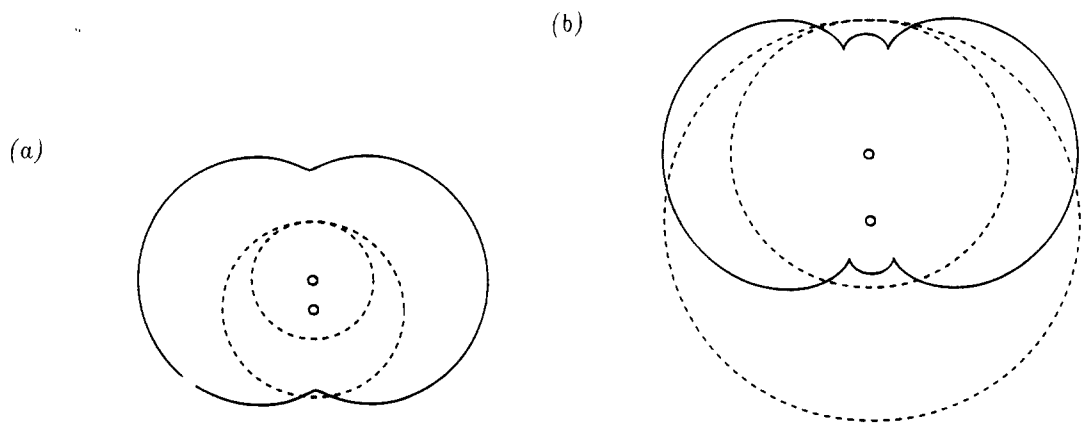

Fig. 15. Examples of singularity of Wankel's chamber. (a) $\lambda = 1.454$, $\rho/r = 0.1333$, (b) $\lambda = 1.454$, $\rho/r = 0.1333$.

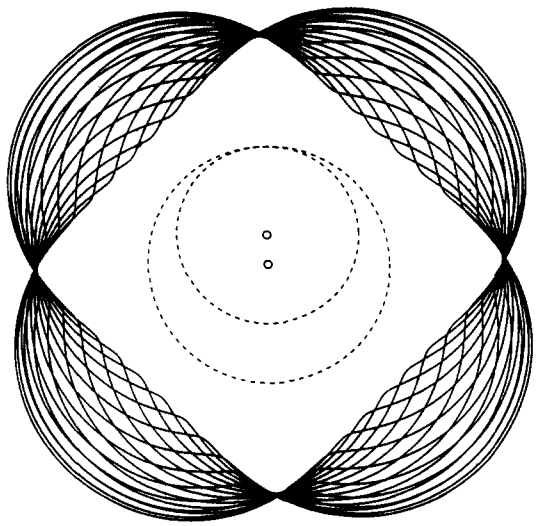

Fig. 16. Example of swept out space: internal tangency of pin and generated curve.

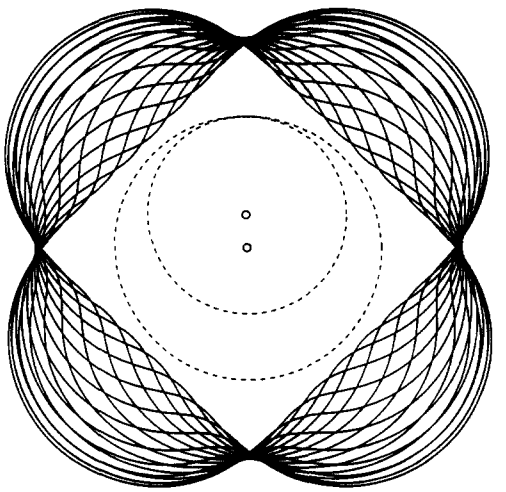

Fig. 17. Examples of swept out space: internal tangency of pin and generated curve.

6. SPACE SWEPT OUT BY GENERATED SHAPE

We consider in this section that profile Σ_2 of the generated shape has been determined and represented in coordinate system S_2. The goal is to determine space Σ_1' that is swept out in S_1 by curve Σ_2. The solution to this problem is based on the following considerations:

(1) We set up the same coordinate systems S_1, S_2, and S_f that have been applied in Section 3 for the generation of Σ_2. It is assumed that links 1 and 2 perform rotation about O_1 and O_2 with the same ratio m_{21}. Thus, there will be the same centrodes and the instantaneous center of rotation as discussed above.

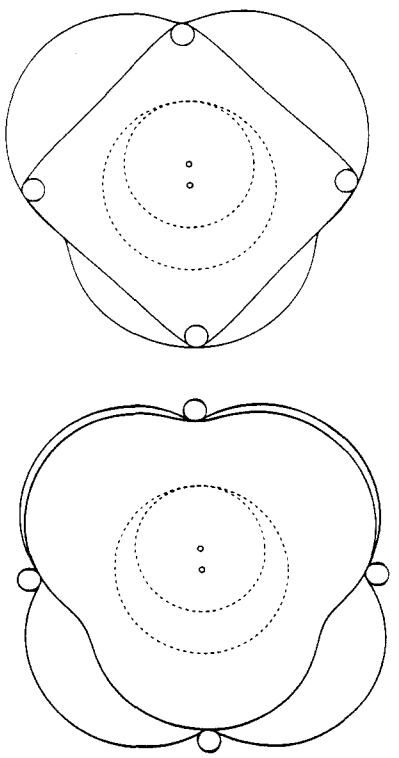

Fig. 18. Examples of connection of pins.

(2) Curve Σ_2 generates in S_1 a family of curves as shown in Figs 16 and 17. Using an approach similar to that discussed above, we are able to determine the envelope Σ_1' to the family of curves Σ_2 represented in S_1. Drawings in Fig. 18 show the envelopes Σ_1' for two cases, when profile Σ_2 is generated by pin Σ_1 being in internal and external tangency with Σ_2, respectively. The envelope consists of two branches that determine the borders of the swept out space. One of the branches of the respective couple of curves Σ_1' can be used for connections of the pins as shown in Fig. 18. It is not excluded the appearance of singular points on one of the branches of Σ_1' as shown in Figs 16 and 17.

The analytical determination of envelope Σ_1' to the family of curves Σ_2 is based on the following procedure:

Step 1: We represent curve Σ_2 in S_2 by the equations (see Section 3)

$$\mathbf{r}_2 = \mathbf{r}_2(\theta, \phi), \quad f(\theta, \phi) = \sin(\theta + \phi) - \lambda \sin\theta = 0 \tag{64}$$

Step 2: The family of curves Σ_2 is represented in S_1 by the equations

$$\mathbf{r}_1(\theta, \phi, \psi) = M_{12}(\psi)\mathbf{r}_2(\theta, \phi), \quad f(\theta, \phi) = 0 \tag{65}$$

Here: ψ_2 and ψ_1 represent the angles of rotation of Σ_2 and Σ_1 about centers O_2 and O_1, where

$$\psi_2 = \psi_1 m_{21}$$

Matrix $M_{12}(\psi)$ is similar to matrix $M_{12}(\phi) = M_{21}^{-1}(\phi)$ [see equation (4) for $M_{21}(\phi)$].

Step 3: To determine the envelope Σ_1' to the family of curves Σ_2, we need the equation of meshing that can be derived as follows

$$\frac{X_2(\psi) - x_2(\theta, \phi)}{n_{x_2}(\theta, \phi)} = \frac{Y_2(\psi) - y_2(\theta, \phi)}{n_{y_2}(\theta, \phi)} \tag{66}$$

Here: $X_2(\psi)$ and $Y_2(\psi)$ represent the coordinates of instantaneous center of rotation I in coordinate system S_2.

Equations (66) yield the equation of meshing between Σ_2 and Σ_1 in the form

$$F(\theta, \phi, \psi) = \sin(\theta + \phi_1 - \phi_2 + \psi_2) - \sin(\theta + \phi_1) = 0 \tag{67}$$

We take into account that equation (67) yields

(i) $$\psi_2 - \phi_2 = 2\pi n \tag{68}$$

(ii) $$\sin(\theta + \phi_1 - \phi_2 + \psi_2) = \sin[(2n + 1)\pi - \theta - \phi_1] \tag{69}$$

where $n = 0, 1, 2, \ldots$

It results from equations (68) and (69) that equation of meshing (67) yields two solutions for ψ_2

(i) $$\psi_2 = \phi_2 + 2\pi n \tag{70}$$

(ii) $$\psi_2 = \phi_2 + (2n + 1)\pi - 2(\theta + \phi_1) \tag{71}$$

Equations (70) and (71) correspond to two branches of the envelope Σ_1', respectively.

Step 4: Equations (65) and (67) represent the sought-for envelope Σ_1'.

7. GENERATION OF CHAMBER WITH TOOL OF INCREASED DIAMETER

Our goal is to generate the chamber by a tool whose diameter is increased with respect to the pin.

Figure 19 shows circles of radii ρ_1 and ρ_2 that represent the original pin and the applied tool, respectively. The circles are in tangency at point M, that passes through centers C_1 and C_2 of the circles, and the instantaneous center of rotation I. Thus, M is the current generating point of the pin and the tool.

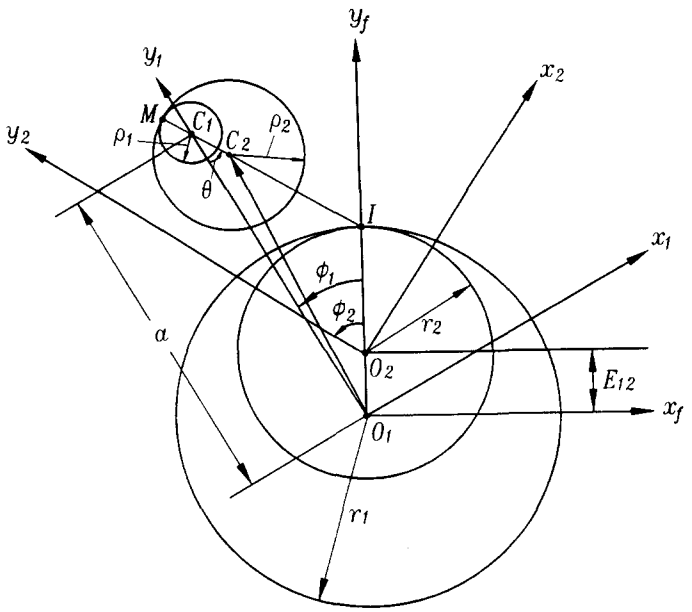

Fig. 19. For generation of chamber with enlarged tool diameter.

The imaginary process of the generation of the chamber is based on the following consideration:

(1) We assume that coordinate system S_1 with the original pin performs rotation about O_1 while coordinate system S_2 with the chamber performs rotation about O_2. The positions of coordinate systems S_1 and S_2 are determined with angles ϕ_1 and ϕ_2 related as follows

$$\frac{\phi_2}{\phi_1} = \frac{r_1}{r_2} \quad (\phi_1 \equiv \phi) \tag{72}$$

The center distance E_{12} is determined as $E_{12} = r_1 - r_2$.

(2) Angle θ that determines the orientation of the contact normal $\overline{MI}$ with respect to $\overline{O_1C_1}$ is determined with equations (25) and (26).

(3) Drawings of Fig. 19 yield that position vector $\overline{O_1C_2}$ is determined in S_1 as

$$x_1^{(C_2)} = (\rho_2 - \rho_1)\sin\theta, \quad y_1^{(C_2)} = a - (\rho_2 - \rho_1)\cos\theta \tag{73}$$

(4) Using coordinate transformation from S_1 to S_2, we obtain the coordinates of center C_2 in coordinate system S_2

$$\mathbf{r}_2^{(C_2)} = M_{21}(\phi)\mathbf{r}_1^{(C_2)}(\theta) \tag{74}$$

where θ and ϕ are related with equation (17). Functions $x_2^{(C_2)}(\phi)$ and $y_2^{(C_2)}(\phi)$ represent in S_2 the current position of the center of the generating circle of radius ρ_2.

The limitation of the described method of generation is that the radius of the increased generating pin cannot be larger than the smallest radius of the curvature of the generated curve. In the case of internal tangency, the limitation of the tool radius can be obtained from equation (50) by considering $\phi = 180°$ as

$$\rho_{\text{limit}} = \frac{r_1(m_{21} - 1)(\lambda + 1)^2}{m_{21} + (m_{21} - 1)\lambda} + \rho \tag{75}$$

Similarly, in the case of external tangency, the limitation of the tool radius can be obtained from equation (50) by considering $\phi = 0°$ as

$$\rho_{\text{limit}} = \frac{r_1(m_{21} - 1)(\lambda - 1)^2}{m_{21} - (m_{21} - 1)\lambda} - \rho \tag{76}$$

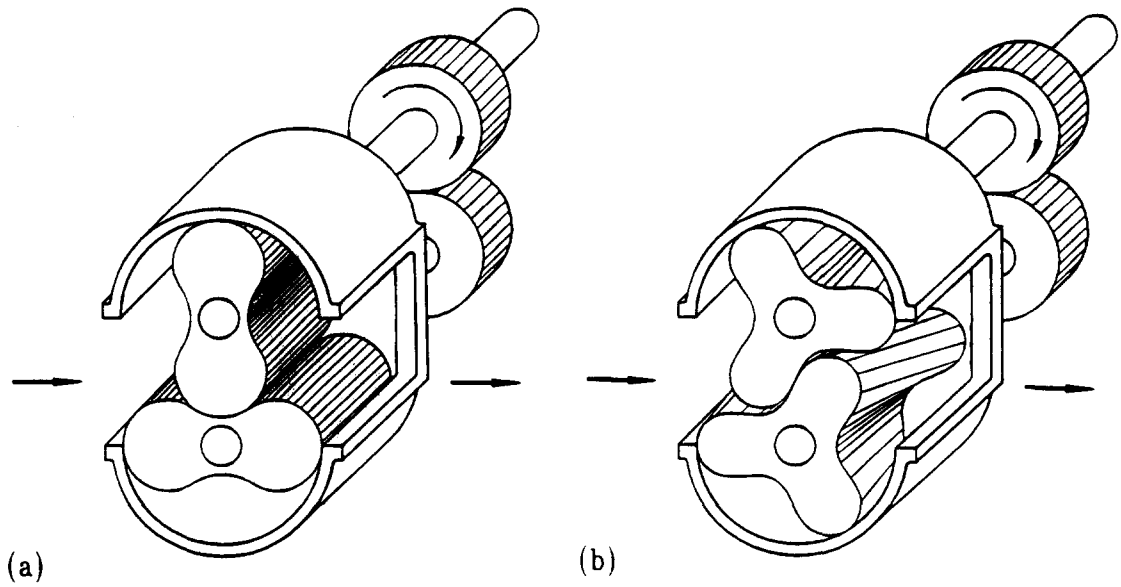

Fig. 20. Root's blower.

8. ROOT'S BLOWER

8.1. Introduction

The Root's blower is designed as a mechanism with two rotors that perform rotation about parallel axes (Fig. 20). The rotors are provided with two lobes [Fig. 20(a)] or with three screw lobes [Fig. 20(b)]. In the last case the surfaces of rotors are helicoids. The main attention in this section is paid to the design of three-lobed rotors.

The axodes of the rotors are two cylinders of equal radius r that are in external tangency. The cross-section of three-lobe rotors is represented in Fig. 4(b). The addendum of the profile is a circle of radius ρ. the dedendum is a curve that is conjugated to the addendum.

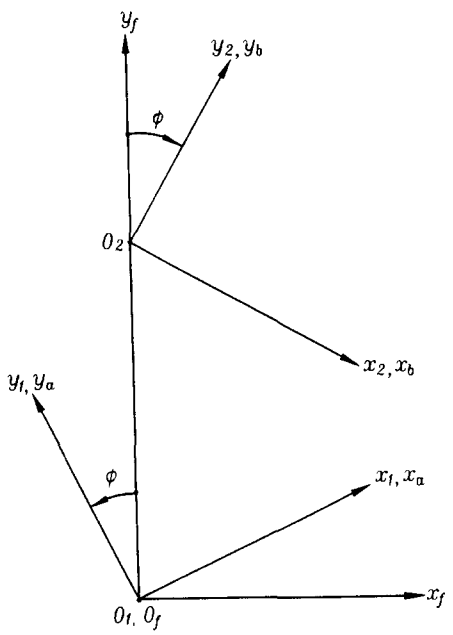

Fig. 21. Coordinate systems applied for Root's blowers.

8.2. Applied coordinate systems

Movable coordinate systems, S_1 and S_2, are rigidly connected to rotors 1 and 2 (Fig. 21). The fixed coordinate system S_f is rigidly connected to the frame of the blower.

8.3. Addendum and dedendum surfaces

Initially we consider the meshing of rotors in plane $z_1 = z_2 = 0$, as meshing of planar curves. The cross-section σ_1 of the addendum surface for a three-lobe rotor is represented in an auxiliary coordinate system S_a by the following equations

$$x_a = \rho \sin\theta, \quad y_a = a + \rho \cos\theta \tag{77}$$

$$-\frac{(a+\rho)^2 - r^2}{\sqrt{2}ar} \leqslant \tan\frac{\theta}{2} \leqslant \frac{(a+\rho)^2 - r^2}{\sqrt{2}ar} \tag{78}$$

The conjugated curve σ_2 will be represented in coordinate system S_b that performs rotational motion about O_2. The rotation of coordinate systems S_a and S_b is considered as similar to rotation of S_1 and S_2 (Fig. 21).

8.4. Equation of meshing

Using the approach similar to that applied in Section 3, we obtain that the equation of meshing of σ_1 and σ_2 is represented as

$$f(\theta, \phi) = r \sin(\theta - \phi) - a \sin\theta = 0 \tag{79}$$

Using the coordinate transformation from S_a to S_b, we obtain that curve σ_2 is represented in S_b by the equations

$$\begin{aligned} x_b &= \rho \sin(\theta - 2\phi) - a \sin 2\phi + 2r \sin\phi \\ y_b &= \rho \cos(\theta - 2\phi) + a \cos 2\phi - 2r \cos\phi \\ & r \sin(\theta - \phi) - a \sin\theta = 0 \end{aligned} \tag{80}$$

The addendum surface Σ_1 of the rotor 1 is a helicoid that is generated by the screw motion of coordinate system S_a with respect to S_1. A right-hand helicoid of the addendum is represented by the equations

$$\begin{aligned} x_1(\theta, \psi) &= \rho \sin(\theta - \psi) - a \sin\psi \\ y_1(\theta, \psi) &= \rho \cos(\theta - \psi) + a \cos\psi \\ z_1(\psi) &= p\psi \end{aligned} \tag{81}$$

Surface Σ_2 of the dedendum of rotor 2 is a helicoid whose direction is opposite to the direction of the helicoid of rotor 1. Surface Σ_2 is generated by the screw motion of curve σ_2 about the axis of rotor 2, and is represented in S_2 as follows

$$\mathbf{r}_2(\theta, \psi, \phi) = M_{2b}(\psi)\mathbf{r}_2(\theta, \phi), \quad f(\theta, \phi) = 0 \tag{82}$$

Equations (82) represent Σ_2 in the three-parameter form but parameters (θ, ϕ) are related.

8.5. Equation of meshing between Σ_1 and Σ_2

We obtain the equation of meshing as

$$\mathbf{N}_1 \cdot \mathbf{v}_1^{(12)} = f(\theta, \psi, \phi) = 0 \tag{83}$$

where $\mathbf{N}_1$ is the normal to surface Σ_1, $\mathbf{v}_1^{(12)}$ is the relative (sliding) velocity. Vectors $\mathbf{N}_1$ and $\mathbf{v}_1^{(12)}$ are represented in S_1 by the following equations

$$\mathbf{N}_1 = \frac{\partial \mathbf{r}_1}{\partial\theta} \times \frac{\partial \mathbf{r}_1}{\partial\psi_1} = \begin{bmatrix} p\rho \sin(\theta - \psi) \\ p\rho \cos(\theta - \psi) \\ \rho a \sin\theta \end{bmatrix} \tag{84}$$

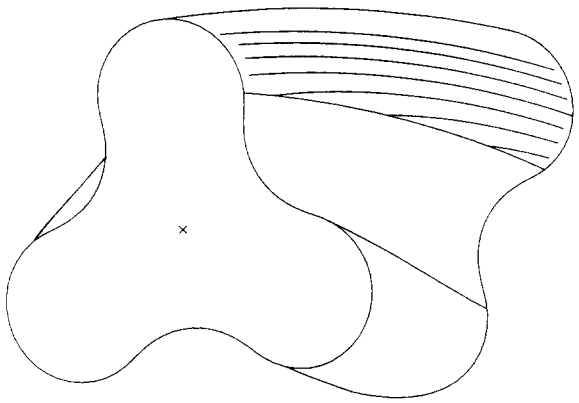

Fig. 22. Contact lines on Root's blower surface.

Table 1. Properties of Σ_2

Lobe number	Convex	Concave–convex	With singularities
2	$0 < \lambda \leqslant 0.5$	$0.5 < \lambda < 0.928822$	$\lambda \geqslant 0.928822$
3	$0 < \lambda \leqslant 0.5$	$0.5 < \lambda < 0.96693$	$\lambda \geqslant 0.96693$

$$\mathbf{v}_1^{(12)} = \begin{bmatrix} -2\omega[\rho\cos(\theta-\psi) + a\cos\psi - r\cos\phi] \\ 2\omega[\rho\sin(\theta-\psi) - a\sin\psi - r\sin\phi] \\ 0 \end{bmatrix} \tag{85}$$

After derivations, we obtain

$$f(\theta, \psi, \phi) = r\sin(\theta - \psi - \phi) - a\sin\theta = 0 \tag{86}$$

Equations (82), if considered simultaneously, allow to obtain the instantaneous lines of contact between Σ_1 and Σ_2 on surface Σ_1 as shown in Fig. 22.

8.6. Properties of σ_2

The planar curve σ_2 may be a convex curve, concave–convex one, with or without singularities depending on the ratio of $\lambda = a/r$. The results of investigation are represented in Table 1.

9. CONCLUSION

The modern theory of gearing for the design of trochoidal gearings has been applied.

(1) Equations of trochoidal and equidistant curves in parametric form have been derived (Sections 2 and 3).

(2) Curvature of trochoidal curves and inflection and stationary points of such curves have been derived (Section 4).

(3) Conditions for avoidance of singularities of generated trochoidal curves have been determined (Section 5).

(4) Space swept out by the generated curve has been determined (Section 6).

(5) Generation of the chamber of Wankel's engine by application of a tool with an increased diameter has been developed (Section 7).

(6) Design of Root's blower with screw rotors has been developed (Section 8).

Acknowledgement—The authors are grateful to the Gleason Memorial Fund for the financial support of this research.

REFERENCES

1. F. L. Litvin, *The Theory of Gearing*, 2nd Edition. Nauka, Moscow (1968).
2. F. L. Litvin, *Theory of Gearing*. NASA RP-1212 (AVSCOM 88-C-035), Washington, D.C. (1989).
3. F. L. Litvin, *Gear Geometry and Applied Theory*. Prentice Hall, Englewood Cliffs, NJ (1994).

4. R. F. Ansdale, with a special contribution by D. J. Lockley, *The Wankel RC Engine*. Barnes and Co., Cranbury, NJ (1969).
5. J. E. Beard, D. W. Yannitell and G. R. Pennock, *Mech. Mach. Theory* **27**, 373 (1992).
6. F. Wankel, *Rotary Piston Machines*. Iliffe Books, London (1963).
7. K. Yamamoto, *Rotary Engine*. Toyo Kogyo, Tokyo (1981).
8. J. E. Beard, A. S. Hall and W. Soedel, *13th Annual ASME Design Autom Conf.*, Vol. 10-2, pp. 355 (1987).
9. J. E. Beard, G. R. Pennock and M. M. Stanisic, *Trans. SAE, J. Comm. Vehicles*, Sec. 2, Vol. 98, pp. 217 (1989).
10. J. R. Colbourne, *Mech. Mach. Theory* **9**, 421 (1974).
11. I. A. Sakun, *Screw Compressors*. Mashinostrojenie, Leningrad (1970) (in Russian).
12. E. A. Dijksman, *Motion Geometry of Mechanisms*. Cambridge Univ. Press, Cambridge (1976).

РЕЭЮМЕ—Рассматривается образование циклоидальных (трохоидальных) зацеплений, нашедших применение в двигателях Ванкеля (Wankel), воздуходувках Рута (Roots) и насосах. Содержание статьи посвящено: (а) образованию и геометрии плоских циклоидаьных зацеплений, винтовых роторов воздуходувок Рута, (б) усовершенствованию проектирования, позволяющего избежать особенностей образуемых кривых и поверхностей. Разработаны компьютерные программы для численных расчётов в дополнение к предложенным аналитическим решениям. Приводятся численные примеры для иллюстрации предложенных методов.